Optical constants of sputtered beryllium thin films determined from photoabsorption measurements in spectral range 20.4–250 eV

Authors

Mikhail Svechnikov[a]*, Nikolay Chkhalo[a], Alexey Lopatin[a], Roman Pleshkov[a], Vladimir Polkovnikov[a], Nikolay Salashchenko[a], Franz Schäfers[b], Mewael G. Sertsu[b], Andrey Sokolov[c] and Nikolay Tsybin[a]

[a] Institute for Physics of Microstructures, Academicheskaya 7, Nizhny Novgorod, 603087, Russian Federation

[b]Department of Nanooptics and Technology, Helmholtz-Zentrum Berlin, Albert-Einstein-Straße 15, Berlin, D-12489, Germany

[c]Department Precision Gratings, Helmholtz-Zentrum Berlin, Albert-Einstein-Straße 15, Berlin, D-12489, Germany

Correspondence email: svechnikovmv@gmail.com

Funding information Russian Foundation for Basic Research (RFBR) (grant No. 19-07-00173; grant No. 19-02-00081; grant No. 18-02-00588; grant No. 17-52-150006; grant No. 18-42-520007; grant No. 18-32-00671; grant No. 18-32-00173); State Assignment for the Institute for Physics of Microstructures, Russian Academy of Sciences (contract No. 0035-2014-0204).

Synopsis The complex refractive index of beryllium was experimentally determined in the spectral range of 20.4–250 eV from transmission spectra of free-standing thin films; a comparison of the found optical constants of beryllium with those obtained earlier in another research group is performed.

Abstract In this work, the refractive index of beryllium in the photon energy range of 20.4–250 eV was experimentally determined. The initial data include measurements of the transmittance of two free-standing Be films with thicknesses of 70 nm and 152 nm, as well as reflectometric measurements of similar films on a substrate. Measurements were carried out at BESSY-II synchrotron radiation source at the Optics beamline. The absorption coefficient β was found directly from the transmission coefficient of the films, and the real part of the polarizability δ was calculated from the Kramers-Kronig relations. A comparison is made with the results obtained 20 years ago at the ALS synchrotron using a similar methodology is performed.

Keywords: beryllium; optical constants; refractive index; photoabsorption; near edge X-ray absorption fine structure spectroscopy; freestanding thin film.

1. Introduction

Beryllium is an important material in X-ray optics, with high transparency in a number of spectral ranges. It is widely used as a material for windows of vacuum chambers, allowing output of X-ray radiation, refractive lenses of synchrotron channels, allowing flexible control of the beam focusing, substrates for X-ray optical elements with high elasticity and thermal conductivity with a small mass (Beguiristain *et al.*, 2002; Chkhalo, Mikhailenko *et al.*, 2019; ESRF). In the extreme ultraviolet wavelength range (EUV), at energies below the K-absorption edge of 111.75 eV, Be is one of the few transparent materials. For this reason (as well as due to the relatively high melting point – 1278 °C for bulk material) it can be used in absorption filters (Chkhalo *et al.*, 2016) and as a component of highly reflective multilayer mirrors for a number of spectral ranges: W/Be mirrors for 0.67–3.12 nm (Akhsakhalyan *et al.*, 2019), Mo/Be for 11.4 nm (solar astronomy and lithography) (Bogachev *et al.*, 2016; Montcalm *et al.*, 1998), Mo/Be/Si for 13.5 nm (solar astronomy and lithography) (Chkhalo, Gusev *et al.*, 2017), Be/Al for 17.1–19 nm and 30.4 nm and Be/Si/Al for 17.1–19 nm (solar astronomy) (Chkhalo, Pariev *et al.*, 2017; Chkhalo, Lopatin *et al.*, 2019), Ti/Be for 25 nm (Chkhalo *et al.*, 1995), Be/Mg for 30.4 nm (solar astronomy) (Polkovnikov *et al.*, 2019). Knowledge of the optical constants (the real and imaginary parts of the refractive index) is necessary to simulate the optical properties and to carry out reflectometric diagnostics of Be-containing optical elements. The most accurate experimental measurement of photoabsorption in thin Be films in the energy range 40–250 eV was performed by (Soufli *et al.*, 1999); these data are available in the database of optical constants (CXRO)(http://henke.lbl.gov/optical_constants/). Prior to this, measurements were performed in the vicinity of the Be absorption edge, 110–170 eV (Haensel *et al.*, 1970), as well as measurements at individual spectral points (Barstow *et al.*, 1983), the rest of soft X-ray (SXR) and EUV range described by calculations (Henke *et al.*, 1993). However, the processing of experimental reflectometric curves often revealed a significant discrepancy with simulation results using CXRO constants in the low-energy region, in particular, to describe Be/Mg mirrors at a wavelength of 30.4 nm (40.78 eV) (Polkovnikov *et al.*, 2019). The reasons for this discrepancy may be incorrect assumptions about the structure and chemical composition of the contaminated surface layer, errors in the thicknesses and roughness of the internal layers, as well as the difference between real optical constants and tabulated ones. To exclude the last factor, it was decided to measure the refractive index of Be in the EUV and SXR ranges, similar to (Soufli *et al.*, 1999). Among other things, the availability of an alternative dataset obtained by a similar technique increases the reliability of tabulated optical constants in the selected energy range.

In this paper, we followed the methodology developed in the works of (Delmotte *et al.*, 2018; Soufli *et al.*, 2019). The thickness of the films and oxide layers were determined by the EUV

reflectometry and checked by transmission modeling. The method of free-standing film transmission measurements in a wide spectral wavelength range was chosen to determine the optical constants, since in this case, the interpretation of the measurement results does not depend on the quality of the interfaces of the films, and the effect of surface contamination (mainly oxidation) can be compensated in a very simple way.

2. Experimental section

2.1. Be films deposition

The Be films were deposited in a specially certified laboratory in IPM RAS since the beryllium is a highly toxic material. Only beryllium dust constitutes a threat to human health and its effect has an accumulating nature. So, according to the sanitary norms, storage, research and long-term operation with the Be-containing films are not harmful to human health; these activities do not require special precautions.

Deposition was carried out by a direct current magnetron sputtering at the facility, pumped out to a residual pressure of 4×10^{-5} Pa. The working pressure of argon during the deposition was 0.11 Pa, and the chemical purity of Ar was about 99.99%. The target materials were disks of diameter 150 mm and thickness 5 mm. The process utilized 270 W of power for the Be target and 160 W for the Mg target.

The films were deposited on a Si wafer with a diameter of 100 mm with a microroughness of less than 0.2 nm. Beryllium was sputtered on top of a 152 nm thick magnesium sacrificial layer. After deposition, the substrate was divided into several parts. For the manufacture of free-standing films, the sacrificial Mg layer was dissolved in acetic acid. For reflectometric measurements, we used films on the substrate.

2.2. EUV and SXR measurements

Reflectivity and transmissivity measurements in the EUV and SXR region were carried out using at-wavelength metrology equipment, with an 11-axis reflectometer end station on the optics beamline of a BESSY-II synchrotron radiation source (Schäfers *et al.*, 2016; Sokolov *et al.*, 2016). The reflectometer is located at the end of the Optics Beamline and is designed specifically for the metrology of the optical elements of the SXR and EUV range at working wavelengths. The range of wavelengths available at this station is 0.62–124 nm (10–2000 eV). The monochromatization of the beam is carried out with a SX-700 monochromator with a replaceable flat grating (it can be switched between two installed gratings of 1200 and 150 lines/mm). The spectral resolution $E/\Delta E$ = 2000–5000, the accuracy of setting the wavelength is 0.02%, the spectral impurities are less than 0.01%. Polarization is variable, from linear to elliptical. The energy scale is calibrated along the edges of the absorption of thin-film filters and along the absorption lines of gases. To suppress high orders, a four-

mirror system operating in the field of total external reflection is used (high order suppressor – HiOS). The reflectometer is equipped with an 11-axis goniometer, angle setting accuracy – 0.02°. The size of the incident beam in this experiment was about 0.6 mm×0.25 mm (width×height). The active area of the detector of 4×4 mm^2 was sufficient to receive specular reflection and most of the scattered part of reflected beam.

Measurements of the spectral and angular reflection curves from films on substrates were carried out with a grating of 1200 lines/mm. The transmission coefficient of the films was measured in the energy range of 14–630 eV, but only part of this range (namely, 20.4–250 eV) was used to extract optical constants; about the reasons for this, we say further. For measurements in the range of 14–110 eV, a grating with 150 lines/mm was used, and for the range of 36–630 eV, 1200 lines/mm was used. In the intersection area, the data was stitched. Calibration was performed at the edges of the absorption of thin-film filters Al, Mg, Si, Be, B, Fe, Ti, Cr, Cu. HiOS mirrors were uncoated bulk Si or had C or AlF_3 coating; the grazing angle for them was 3–40°, depending on the energy. Absorption filters were not used in the measurement process.

3. Beryllium thin films

The thickness of the Be films, as well as the thickness of the oxide layer of BeO, which forms on the surface in normal conditions, were determined from the results of measurements of the reflection and transmission coefficients. The reflection curves were measured for Be-on-Mg films on substrate. Thus, the study involved 4 samples, which are schematically shown in Fig. 1. Samples PR150film and PR152film are free-standing films corresponding to samples PR150 and PR152 after dissolving the Mg layer in an aqueous solution of acetic acid. After dissolving the Mg layer, the Be films were caught on frames with a through hole with a diameter of 8 mm. As revealed by subsequent measurements of the transmission spectra, no jumps in the region of the Mg-$L_{2,3}$ absorption edges (49.5–49.9 eV) were observed, which means there is no residual Mg on the free-standing samples.

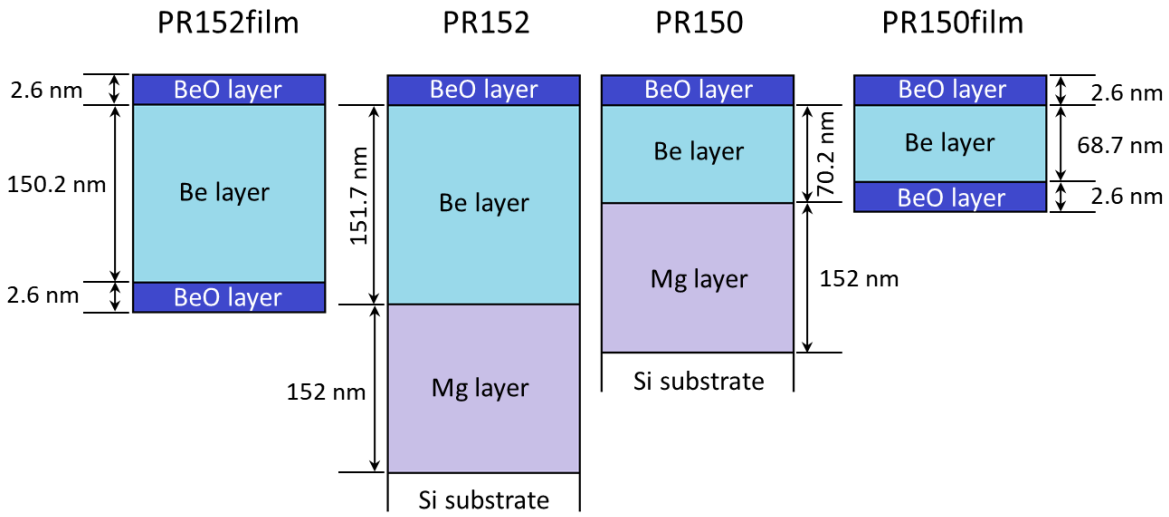

Figure 1 Schematic structure of samples on substrates and free-standing films. The shown Mg layer thickness is nominal, the Be and BeO thicknesses are determined according to the reflectometry of the samples on the substrates and the transmission measurement of free-standing films.

The thickness of the "pure" Be core layer and the natural surface oxide film BeO was determined by reflectometric reconstruction. Also, according to the results of reflectometric modeling, it was found that the interlayer roughness in the structures on the substrate is about 4.5 nm (in root-mean-square sense). Such a large value is apparently due to the growth roughness of the thick "sacrificial" layer of Mg. The difference in the thickness of the Be layer in the samples on the substrate and free-standing films is associated with the appearance of an oxide film on the reverse side. At nominal densities $\rho(\mathrm{Be}) = 1.848$ g/cm^3 and $\rho(\mathrm{BeO}) = 3$ g/cm^3 the formation of 2.6 nm BeO requires about 1.5 nm of "pure" Be. Therefore, the Be layer between two BeO layers in free-standing films is 1.5 nm thinner than the Be layer between BeO and Mg in the films on the substrate.

Fig. 2(a-d) shows the angular and spectral reflectivity curves for "thick" (PR152) and "thin" (PR150) films along with fitted model curves. The simulation was carried out in the program Multifitting (our development, preparing for publication). Both samples were reconstructed simultaneously, with the imposed condition that the thickness and density of the oxide layer BeO were the same for both films. Modelling the transmission curves of free-standing films (first of all, in the region of the K-edge of oxygen) with the same oxide layer approved the consistency of found parameters.

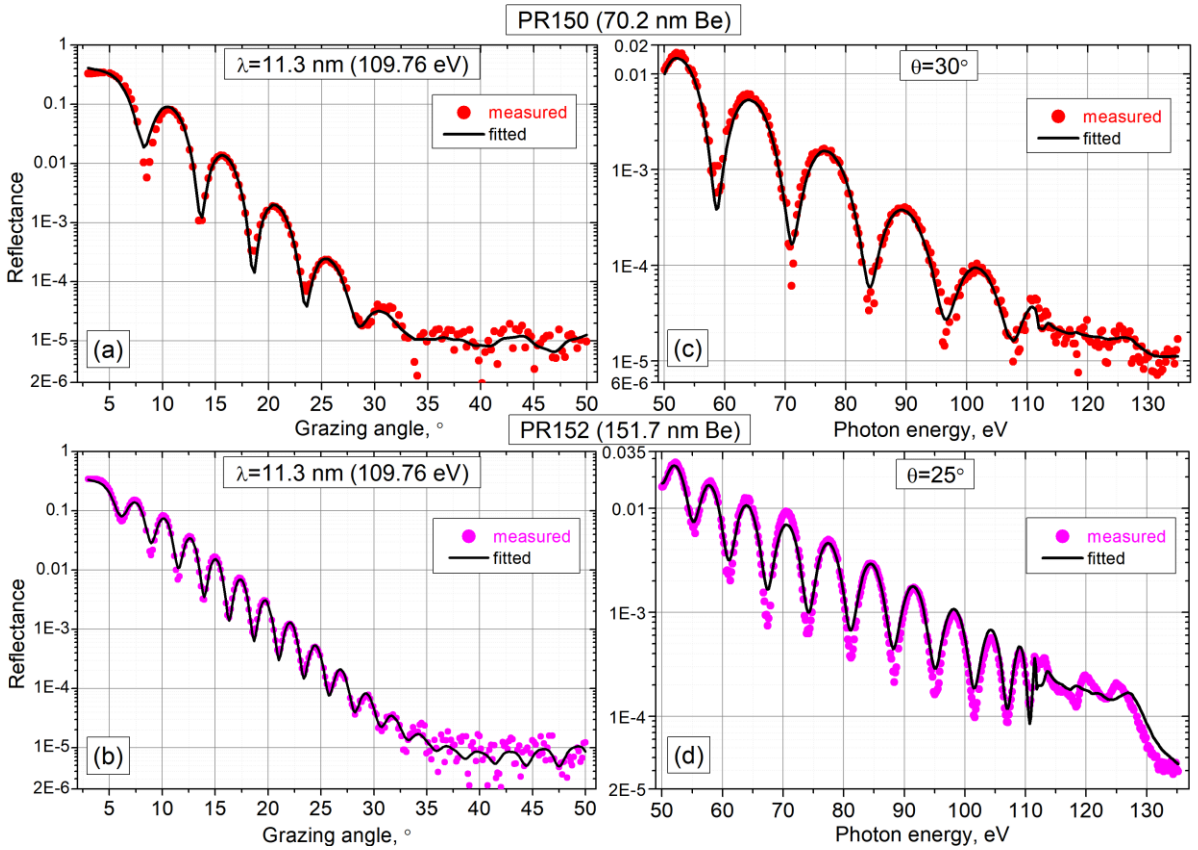

Figure 2 Angular and spectral reflection curves from films on substrates. In Fig. (a) and (b) the wavelength is fixed, in Fig. (c) and (d) the grazing angle of the probe beam is fixed.

4. Transmittance of Be thin films

The transmission curves of free-standing PR150film and PR152film films were measured in the range 14–630 eV as shown in Fig. 3. At the same time, due to the rapidly decreasing intensity of the probe beam to the region of low energies and the increasing absorption of Be, the dynamic range of the Optics Beamline end station does not allow measuring the transmission below ~10^{-3}. For PR150film, the smallest energy value at which the signal noticeably exceeds the noise is 18.5 eV at T≈4.5×10^{-3}, and for PR152film the lower bound is 20.4 eV with T≈9×10^{-4}. The main features of the curves are the structures of the absorption edges of Be-K, C-K and O-K. It is important to note that in spite of the fact that C and O are present in the studied samples in some quantities, they are also present on the surface of the optical elements of the synchrotron beamline. Since this spectrum is present in the incident and transmitted beams, after dividing the transmitted signal by the incident one the absorption spectrum of the channel should be compensated. But the necessary condition for this is the monochromaticity of the incident and transmitted beam, i.e. low intensity of high orders and scattered radiation.

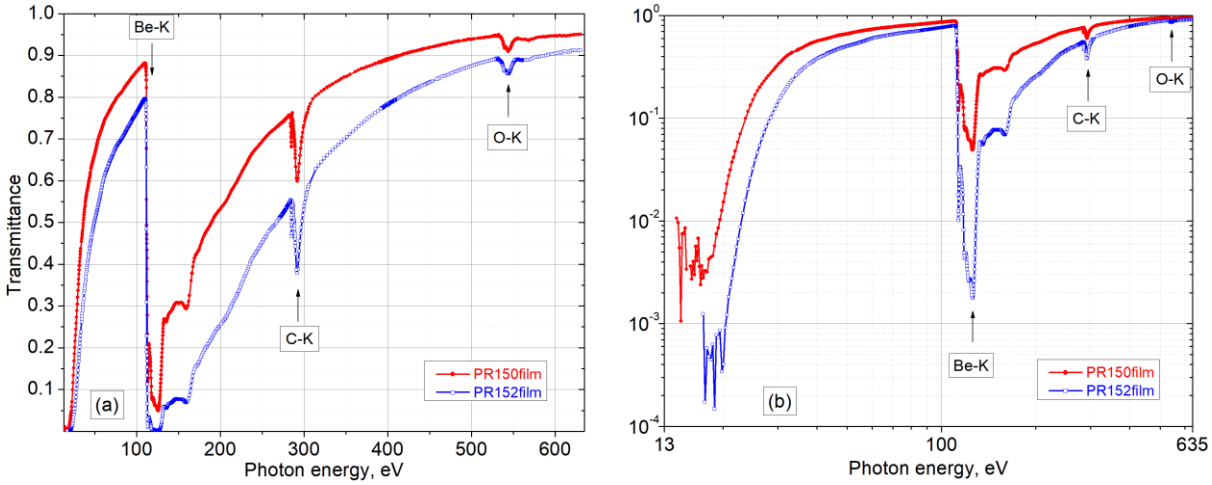

Figure 3 The transmission spectra of the samples at the linear (a) and double logarithmic (b) scale. In the low-energy region, the curves fall to the noise level due to a decrease in the radiation intensity.

If the main diffraction order of grating falls on the region of strong absorption, then after the beam passes the polluted channel, the degree of monochromatization drops sharply and in reality there is a beam with a significant part of spectral impurities. Accordingly, the resulting transmission spectrum of the sample in this area is distorted. In our case, a strong suppression of the main order by the beamline optics occurs in the region of carbon absorption. Fig. 4 shows the signal from the detector when measuring the spectrum in the vicinity of the C-K absorption edge. The intensity of the main

diffraction order corresponding to the monochromatized beam decreases by ~10–200 times in the region of 280–310 eV and exceeds the noise level by only 10–100 times.

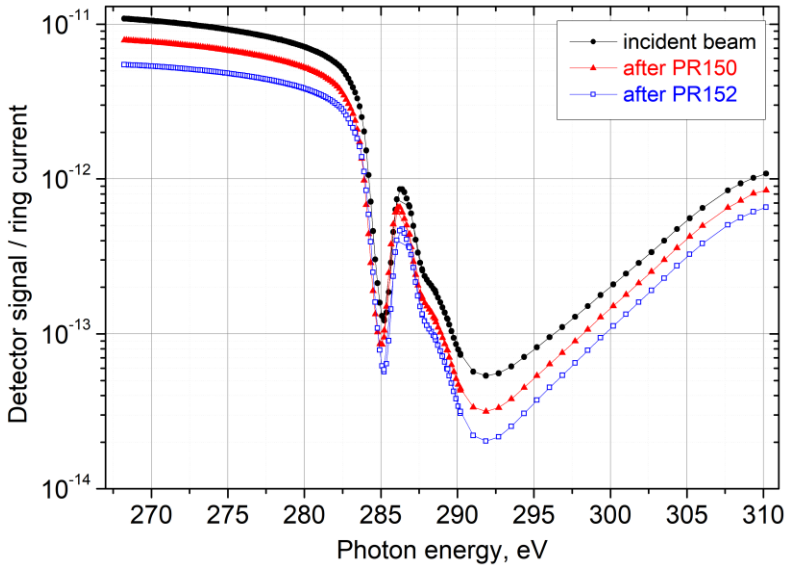

Figure 4 The fall of the signal at the detector when measuring the incident and transmitted beams in the vicinity of the C-K absorption edge.

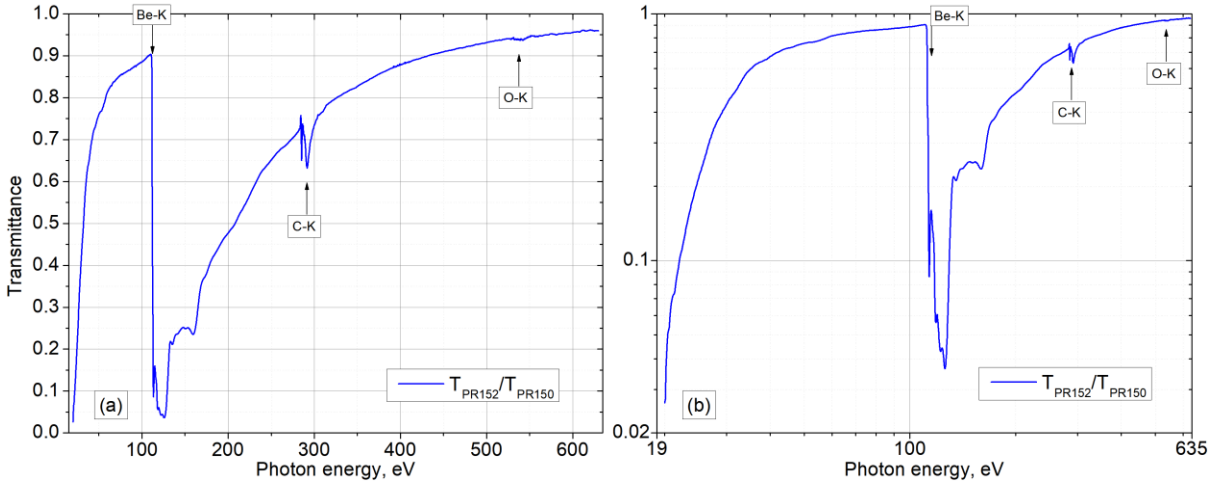

Figure 5 "Differential" transmittance spectrum in linear (a) and double logarithmic (b) scale. This spectrum corresponds to the "ideal" 81.5 nm Be film without surface contamination.

Fig. 5 shows the "differential" spectrum corresponding to the amount of material (and its chemical composition) by which the two free-standing films differ. This spectrum is the ratio of the transmission spectra T_{PR152}/T_{PR150}. Since it is assumed that the surface layers containing the major part of the contamination are the same for both samples, this "differential" film consists of "internal" Be and has a thickness d(PR152film) - d(PR150film) = 150.2 nm - 68.7 nm = 81.5 nm. As can be seen from Fig. 5 (a), compared with the spectra of Fig. 3 (a), the edge of oxygen in the " differential " spectrum almost disappeared. This means that both films PR152film and PR150film contain small

total amount of oxygen in the entire thickness. Incomplete compensation can be associated with the difference in the amount of oxygen inside the Be films of various thickness and is also possible with slight differences in the thickness of the surface oxides. Here we assumed the surface layers fully identical and modeled the "differential" spectrum together with the individual spectra of both samples, as well as reflectometric curves. The simulation showed that the chemical composition of the film thickness, assuming that the main impurities are carbon and oxygen – $Be_1C_xO_y$, where x=0.012–0.020, y=0.003–0.006, i.e. 1.2–2% C and 0.3–0.6% O (atomic concentrations).

The previously mentioned distortion of the spectrum in the region of 280–310 eV leads to the fact that the observed absorption level in the region of C-K edge is much higher than the real absorption associated with carbon impurities inside the sample. Because of this effect, a strong C-K edge is still observed in the "differential" spectrum, but the transmittance modeling in the region of >310 eV does not show a significant amount of carbon in the samples. Since the main goal of this work is to determine the optical constants in the lower energy region, for the reconstruction of the refractive index we used the only spectral region <250 eV, which does not contain such strong distortions like an artifact absorption structure.

5. Determination of Be optical constants

The part of the "differential" spectrum shown in Fig. 5, in the energy range of 20.4–250 eV, is the direct source of data for the imaginary part of the refractive index. The difference spectrum is associated with the linear absorption coefficient of Be α and the absorption of impurities α_{CxOy}:

$$T(E,x) = \exp(-x\alpha(E))\exp(-x\alpha_{C_xO_y}(E)) \quad (1)$$

α_{CxOy} is considered to be known, this data is in the CXRO optical constants database (imaginary parts are down to 10 eV). The thickness x=81.5 nm is defined as the difference between the thicknesses of the studied samples PR152film and PR150film. In expression (1), the beam is implied to be monochromatic; taking into account the high order suppression system based on four mirrors, the contribution of the second and higher diffraction orders can be considered negligible in the target range. The region in the vicinity of C-K, where the monochromaticity condition is not satisfied due to the contamination of the beamline optics and the strong absorption of the main diffraction order, was excluded from consideration. The refractive index $n=1-\delta+i\beta$, the imaginary part β is proportional to α:

$$\beta(E) = \lambda\alpha(E)/4\pi \quad (2)$$

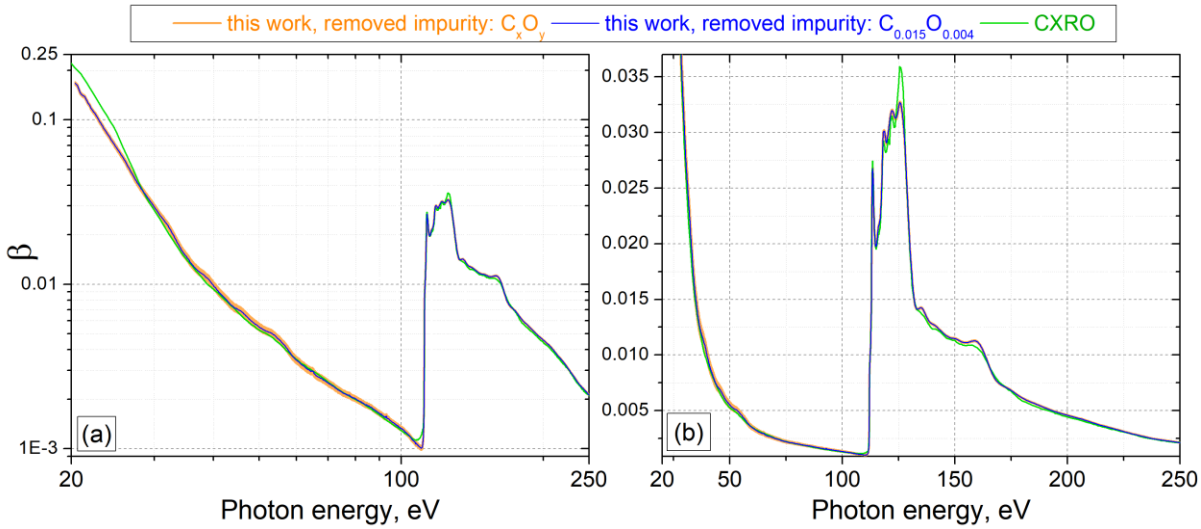

Figure 6 The absorption coefficient β obtained from the spectrum in Fig. 5 in accordance with expression (1), as well as data from the CXRO database. (a) - double logarithmic, (b) – linear scale. The orange area shows the uncertainty (up to ±5%) associated with C content in the range of 1.2–2% and O in the range of 0.3–0.6% (by atomic concentration). Blue line for $C_{x=0.015}O_{y=0.004}$ corresponds to content of 1.5% C and 0.4% O inside Be film.

Depending on the proportion of C and O in the film, an error bar for β was obtained, shown in Fig. 6 in orange color. The uncertainty associated with impurities affects mainly the region up to the absorption edge of beryllium, in the range of 30–111 eV. As can be seen, all the main features of the absorption curve obtained in the work (Soufli *et al.*, 1999) are also found in this study. The differences are only quantitative: in the region of the beginning of the absorption edge, 105.5–111.5 eV, the curve obtained by us has a much sharper appearance; the absorption peak at 123.8–127.5 eV is less pronounced; also in the range of 20–28 eV, the values of β found by us are 5–25% lower than those given in CXRO.

The Kramers-Kronig relations connecting the real and imaginary parts of the complex-valued function can be applied both to the dielectric permittivity and to the refractive index (Nussenzveig, 1972, pp. 17-19). Accordingly, the real part of polarizability can be found using the equation

$$\delta(E) = -\frac{2}{\pi}\int_0^\infty \frac{E'\beta(E')}{E'^2 - E^2}dE' \qquad (3)$$

To find δ in the range of 20.4–250 eV, it is necessary to have β values in a wide range of energies $\{E_{min}, E_{max}\}$, $E_{min} << 20.4$ eV, $E_{max} >> 250$ eV. The following datasets were used: in the range of 0.02–4.2 eV data (Rakić *et al.*, 1998; Polyanskiy), calculated using the Lorentz-Drude model; for 4.2–20.4 eV, the data (Palik, 1991), for 20.4–250 eV, the data obtained in this work, for 250–5950 eV – (CXRO), for 5950–432945 eV – (Chantler). These sources were also used in (Delmotte *et al.*, 2018)

to obtain the optical constants Cr and (Soufli *et al.*, 2019) for Pt. The combined β curve is shown in Fig. 7.

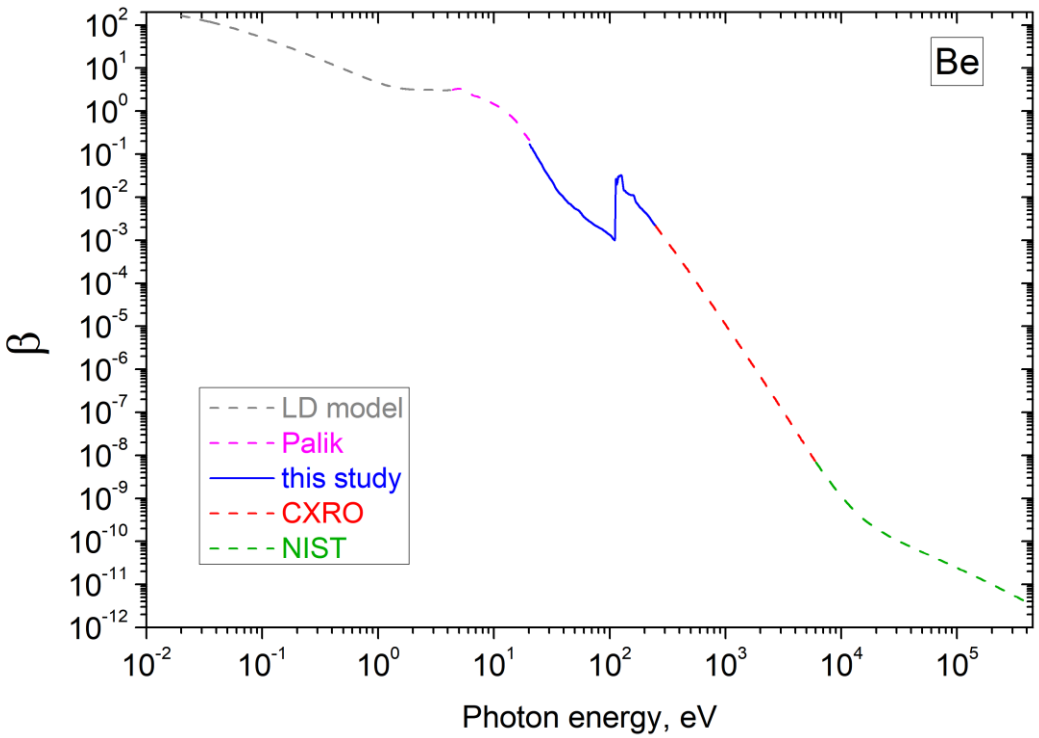

Figure 7 The total data set β, used to calculate δ with the formula (3).

The result of applying the Kramers-Kronig relation is shown in Fig. 8. The difference in the experimentally determined curves β due to the uncertainty of impurities does not have any noticeable effect on the value of δ, therefore Fig. 8 shows only one curve for present study.

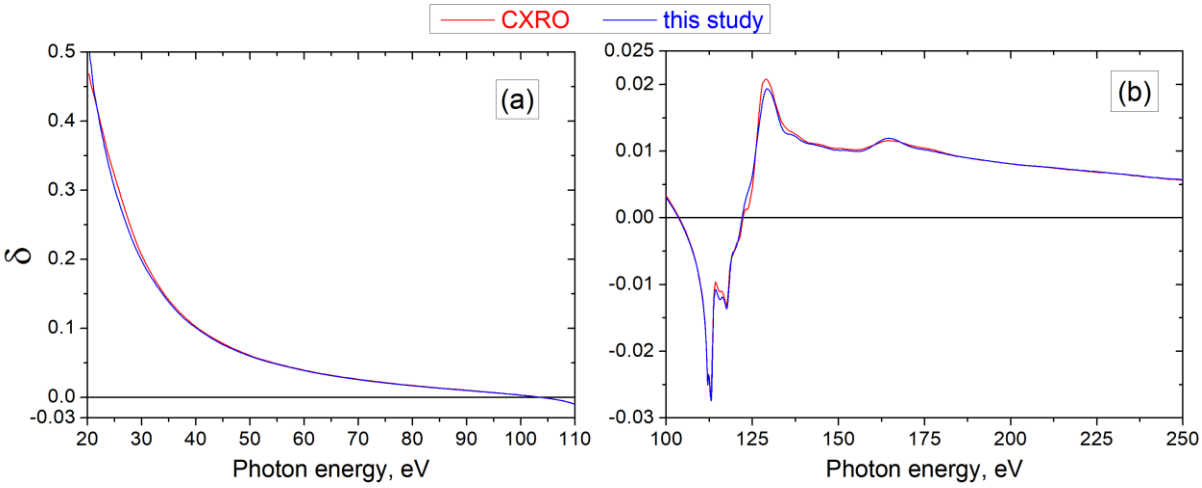

Figure 8 Polarizability δ defined in this paper (blue curve) versus tabulated CXRO data (red curve). The long-wavelength (a) and short-wavelength (b) energy ranges are presented separately.

One of the criteria for the correctness of the found values of β in a wide spectral range is the relation (Rodríguez-de Marcos *et al.*, 2016)

$$N_{eff} = \frac{4m\varepsilon_0}{\pi n_a \hbar^2 e^2} \int_0^\infty E'\beta(E')dE' \quad (4)$$

where $N_{eff} = Z^* = Z - (Z/82.5)^{2.37}$ – effective number of electrons in an atom, n_a – atomic density of the material, m and e – mass and charge of electron respectively, ε_0 – electric constant, $\hbar$ – Planck constant. For Be Z=4, a Z^*=3.999. The closer the value of N_{eff} found by formula (4) to the value of Z^*, the more consistent the set of values of optical constants is. This relation is called the "sum rule".

The effective number of electrons is $N_{eff\ CXRO}$=3.955 using the CXRO data and N_{eff} =3.928 using the optical constants β found by us in the range of 20.4–250 eV. The limits of integration, as with the use of expression (3), were 0.02–433000 eV. The uncertainty of the absorption coefficient associated with the uncertainty of C and O impurities leads to N_{eff} values in the range 3.925–3.931. This variation is significantly smaller than the difference from $N_{eff\ CXRO}$ and, thus, we can assume that in the whole range of 20.4–250, the CXRO data is more consistent with combined wide-range β set. However, we can find out which particular subrange introduces the greatest error in the integral estimate. If, in the calculation, we take the β found by us only from the region of 28–250 eV, and in the region of 20.4–28 eV we take the CXRO data, then N_{eff} =3.969. This means that in the 28–250 eV region, the values we found turn out to be more consistent with the combined data set (shown in Fig. 7) than the CXRO constants, but the values we found in the 20.4–28 eV range turn out to be less consistent. In Fig. 6 (a) it can also be seen the difference between our data and CXRO, increasing with decreasing photon energy. Thus, according to the "sum rule", our data in the region of 20.4–28 eV should be considered as less reliable and CXRO tabulated values should be preferred. There are also technical reasons for this associated with a sharp decrease in the intensity of the monochromatic beam when using a diffraction grating with 150 lines/mm in the low-energy region. In addition to the low dynamic range (about three orders of magnitude), there is a distortion of the spectrum and an increase in the proportion of shorter wavelength radiation, which has a higher transmission through the sample, which, in turn, leads to an underestimation of the found β.

Conclusion

In this paper, the optical constants of Be were determined by measuring the photoabsorption of free-standing films. In addition to oxidized and contaminated surface layers, impurities C in the amount of 1.2–2% and O in the amount of 0.3–0.6% (in atomic concentration) were found in the sample. Two free-standing films with thicknesses of 70 nm and 152 nm were studied for transmission and two corresponding films (with Mg sacrificial layers) on a substrate for reflection. Combining the obtained absorption β with data from the literature in the range of 0.02–433000 eV made it possible to find δ by

the Kramers-Kronig relation, and also to check the obtained set of constants for consistency with the combined set by the criterion of the "sum rules". Thus, the main result of this study is independent confirmation of the reliability of the optical Be constants given in the CXRO database in the photon energy range of 28–250 eV up to fine structure in the Be-K absorption edge. The fine structure of the found optical constants is generally consistent with the CXRO data, but there are quantitative differences. The test for the fulfillment of the "sum rule" showed that at energies of 28–250 eV, the values obtained in this work are more consistent, while at energies of 20.4–28 eV, CXRO data are more consistent. Apparently, this is due to the insufficient efficiency of the diffraction grating used in the experiment in the long-wavelength part of the spectrum, resulting in a strong drop in the intensity of the probe beam.

Acknowledgements This work was supported by the State Assignment for the Institute for Physics of Microstructures, Russian Academy of Sciences, topic no. 0035-2014-0204 and RFBR ## 19-07-00173, 19-02-00081, 18-02-00588, 17-52-150006, 18-42-520007, 18-32-00671 and 18-32-00173.

References

Akhsakhalyan, A. A., Vainer, Y. A., Garakhin, S. A., Elina, K. A., Zavertkin, P. S., Zuev, S. Y., Ivlyushkin, D. V., Nechay, A. N., Nikolenko, A. D., Pariev, D. E., Pleshkov, R. S., Polkovnikov, V. N., Salashchenko, N. N., Svechnikov, M. V. & Chkhalo, N. I. (2019). *J. Surf. Investig. X-Ray, Synchrotron Neutron Tech.* **13**, 1–7.

Barstow, M. A., Lewis, M. & Petre, R. (1983). *J. Opt. Soc. Am.* **73**, 1220.

Beguiristain, H. R., Cremer, J. T., Piestrup, M. A., Gary, C. K. & Pantell, R. H. (2002). *Opt. Lett.* **27**, 778.

Bogachev, S. A., Chkhalo, N. I., Kuzin, S. V., Pariev, D. E., Polkovnikov, V. N., Salashchenko, N. N., Shestov, S. V. & Zuev, S. Y. (2016). *Appl. Opt.* **55**, 2126.

Chantler, C. T. NIST: National Institute of Standards and Technology. http://physics.nist.gov/ffast

Chkhalo, N. I., Drozdov, M. N., Kluenkov, E. B., Kuzin, S. V., Lopatin, A. Y., Luchin, V. I., Salashchenko, N. N., Tsybin, N. N. & Zuev, S. Y. (2016). *Appl. Opt.* **55**, 4683.

Chkhalo, N. I., Fedorchenko, M. V., Kovalenko, N. V., Kruglyakov, E. P., Volokhov, A. I., Chernov, V. A. & Mytnichenko, S. V. (1995). *Nucl. Instruments Methods Phys. Res. Sect. A Accel. Spectrometers, Detect. Assoc. Equip.* **359**, 121–126.

Chkhalo, N. I., Gusev, S. A., Nechay, A. N., Pariev, D. E., Polkovnikov, V. N., Salashchenko, N. N., Schäfers, F., Sertsu, M. G., Sokolov, A., Svechnikov, M. V. & Tatarsky, D. A. (2017). *Opt. Lett.* **42**, 5070.

Chkhalo, N. I., Lopatin, A. Y., Nechay, A. N., Pariev, D. E., Pestov, A. E., Polkovnikov, V. N., Salashchenko, N. N., Schäfers, F., Sertsu, M. G., Sokolov, A. A., Svechnikov, M. V., Tsybin, N.

N. & Zuev, S. Y. (2019). *J. Nanosci. Nanotechnol.* **19**, 546–553.

Chkhalo, N. I., Mikhailenko, M. S., Pestov, A. E., Polkovnikov, V. N., Zorina, M. V., Zuev, S. Y., Kazakov, D. S., Milkov, A. V., Strulya, I. L., Filichkina, V. A. & Kozlov, A. S. (2019). *Appl. Opt.* **58**, 3652.

Chkhalo, N. I., Pariev, D. E., Polkovnikov, V. N., Salashchenko, N. N., Shaposhnikov, R. A., Stroulea, I. L., Svechnikov, M. V., Vainer, Y. A. & Zuev, S. Y. (2017). *Thin Solid Films*. **631**, 106–111.

CXRO : The Center for X-Ray Optics, http://henke.lbl.gov/optical_constants/

Delmotte, F., Meyer-Ilse, J., Salmassi, F., Soufli, R., Burcklen, C., Rebellato, J., Jérome, A., Vickridge, I., Briand, E. & Gullikson, E. (2018). *J. Appl. Phys.* **124**, 035107.

ESRF Focusing compound refractive Beryllium lenses. http://www.esrf.eu/UsersAndScience/Experiments/DynExtrCond/ID28/BeamlineLayout/OH2/FocusBeCRL

Haensel, R., Keitel, G., Sonntag, B., Kunz, C. & Schreiber, P. (1970). *Phys. Status Solidi*. **2**, 85–90.

Henke, B. L., Gullikson, E. M. & Davis, J. C. (1993). *At. Data Nucl. Data Tables*. **54**, 181–342.

Montcalm, C., Bajt, S., Mirkarimi, P. B., Spiller, E. A., Weber, F. J. & Folta, J. a. (1998). *Spie*, Vol. *3331*, edited by Y. Vladimirsky, p. 42.

Nussenzveig, H. M. (1972). Causality and dispersion relations New York, USA: Academic Press.

Palik, E. D. (1991). Handbook of optical constants of solids II Boston: Academic Press.

Polkovnikov, V. N., Chkhalo, N. I., Pleshkov, R. S., Salashchenko, N. N., Schäfers, F., Sertsu, M. G., Sokolov, A., Svechnikov, M. V. & Zuev, S. Y. (2019). *Opt. Lett.* **44**, 263–266.

Polyanskiy, M. N. Refractive index database. https://refractiveindex.info

Rakić, A. D., Djurišić, A. B., Elazar, J. M. & Majewski, M. L. (1998). *Appl. Opt.* **37**, 5271.

Rodríguez-de Marcos, L. V, Méndez, J. A. & Larruquert, J. I. (2016). *J. Opt.* **18**, 075606.

Schäfers, F., Bischoff, P., Eggenstein, F., Erko, A., Gaupp, A., Künstner, S., Mast, M., Schmidt, J. S., Senf, F., Siewert, F., Sokolov, A. & Zeschke, T. (2016). *J. Synchrotron Radiat.* **23**, 67–77.

Sokolov, A., Bischoff, P., Eggenstein, F., Erko, A., Gaupp, A., Künstner, S., Mast, M., Schmidt, J.-S., Senf, F., Siewert, F., Zeschke, T. & Schäfers, F. (2016). *Rev. Sci. Instrum.* **87**, 052005.

Soufli, R., Bajt, S. & Gullikson, E. M. (1999). *Proceedings of SPIE - The International Society for Optical Engineering*, Vol. *3767*, edited by C.A. MacDonald, K.A. Goldberg, J.R. Maldonado, H.H. Chen-Mayer & S.P. Vernon, pp. 251–258.

Soufli, R., Delmotte, F., Meyer-Ilse, J., Salmassi, F., Brejnholt, N., Massahi, S., Girou, D., Christensen, F. & Gullikson, E. M. (2019). *J. Appl. Phys.* **125**, 085106.